CARBON letters

Original Articles
Carbon Letters Vol. 25, 33-42 (2018)

The effect of the modification methods on the catalytic performance of activated carbon supported CuO-ZnO catalysts

Huamei Duan[1,2,3,♠], Yunxia Yang[3,♠], Jim Patel[3], Nick Burke[3], Yuchun Zhai[4], Paul A. Webley[2,♠], Dengfu Chen[1] and Mujun Long[1]

[1]Chongqing University, Chongqing 400044, China
[2]The University of Melbourne, Melbourne 3168, Australia
[3]CSIRO, Melbourne 3168, Australia
[4]Northeastern University, Shenyang 110819, China

Article Info

Received 14 January 2017
Accepted 25 August 2017

♠Corresponding Author
E-mail: duanhuamei@cqu.edu.cn
yunxia.yang@csiro.au
paul.webley@unimelb.edu.au

Open Access

DOI: http://dx.doi.org/10.5714/CL.2018.25.033

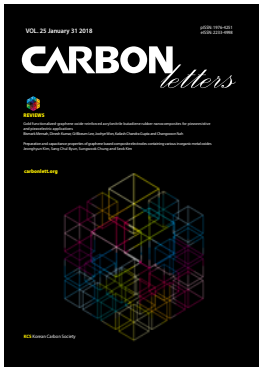

http://carbonlett.org

pISSN: 1976-4251
eISSN: 2233-4998

Abstract

Activated carbon (AC) was modified by ammonium persulphate or nitric acid, respectively. AC and the modified materials were used as catalyst supports. The oxygen groups were introduced in the supports during the modifications. All the supports were characterized by N_2-physisorption, Raman, X-ray photoelectron spectroscopy (XPS), transmission electron microscopy (TEM), and thermogravimetric analysis. Methanol synthesis catalysts were prepared through wet impregnation of copper nitrate and zinc nitrate on the supports followed by thermal decomposition. These catalysts were measured by the means of N_2-physisorption, X-ray diffraction, XPS, temperature programmed reduction and TEM tests. The catalytic performances of the prepared catalysts were compared with a commercial catalyst (CZA) in this work. The results showed that the methanol production rate of AC-CZ (23 mmol-CH_3OH/(g-Cu·h)) was higher, on Cu loading basis, than that of CZA (9 mmol-CH_3OH/(g-Cu·h)). We also found that the modification methods produced strong metal-support interactions leading to poor catalytic performance. AC without any modification can prompt the catalytic performance of the resulted catalyst.

Key words: CO_2 hydrogenation, methanol, activated carbon, supported catalysts, clean energy

1. Introduction

CO_2 has been seen as a hydrogen storage medium through the CO_2 hydrogenation to methanol process [1-3]. Thus, this process has attracted numerous interests during the past decades. Though the synthesis of methanol over $Cu/ZnO/Al_2O_3$ catalyst is a well-established process, there has been ongoing debate around the core catalyst $Cu/ZnO/Al_2O_3$. Fundamental study about new approaches to synthesis more effective catalysts are still one of the hot topics in the current literatures [4-7].

Carbon materials have been used for long as a very attractive catalyst support [8-11]. In the current work, we used the most common carbon material, commercial activated carbon as the catalyst support. These activated carbons have disordered structures consisting of aromatic sheets and strips, usually bent and resembling a mixture of wood shavings and crumpled paper. Those sheets and strips are recognized as the basal planes and the edge of the basal planes are unsaturated carbon atoms which can bond with H or O. Modification by ammonium persulphate (APS) or HNO_3 was introduced to create functional groups on the surface which makes the support accessible to the metal precursors [12-14]. Whether these functional groups beneficial the CO_2 hydrogenation to methanol was still unclear.

We herein present a study on structure and activity of CuO-ZnO particles supported

on activated carbon and modified carbon materials. AC, AC-APS and AC-HNO_3 were used as catalyst supports. The supports were characterized by N_2-physisorption, transmission electron microscopy (TEM), thermogravimetric analysis and Raman analysis. Three CuO-ZnO catalysts were prepared on these supports and were characterized by N_2-physisorption, temperature programmed reduction (TPR), X-ray photoelectron spectroscopy (XPS) and TEM. The effects of the different modification methods of the carbon supports on the catalytic performances of the supported catalysts are analyzed and discussed. The catalytic performances of the three supports and prepared catalysts were compared with a chosen commercial catalyst (CZA).

2. Experimental

2.1. Preparation of supports

The coconut shell type of activated carbon (AC) was supplied by Activated Carbon Technologies Pty Ltd in Australia. The AC was grounded and sieved to 200–300 μm size prior to use. Then two different modifications were applied to achieve carbon surfaces with different properties: (1) AC was treated in 1 M HNO_3 at 373 K for 6 h, followed by extensive washing with distilled water and overnight drying at 373 K. The resulting support was named as AC-HNO_3. (2) AC was treated in 0.1M APS solution at 288 K for 24 h, followed by extensive washing with distilled water and overnight drying at 373 K. The resulting support was named as AC-APS.

2.2. Preparation of catalysts

Reagent grade of $Cu(NO_3)_2{\cdot}2.5H_2O$ and $Zn(NO_3)_2{\cdot}6H_2O$ were purchased from Sigma-Aldrich. The amount of the added salts was based on the total pore volume of AC and the metal loading of the resulting catalysts was 21%. The mole ratio of CuO to ZnO was 2. The support (2 g) was dispersed in absolute ethanol (4.0g), followed by the addition of a 20% alcoholic solution containing of $Cu(NO_3)_2{\cdot}2.5H_2O$ and $Zn(NO_3)_2{\cdot}6H_2O$. The mixture was placed in a rotary evaporator (IKA RV10) with a rotating rate of 100 rpm. After being dried thoroughly at room temperature under vacuum, the sample was put in a tube furnace and calcined under a nitrogen atmosphere at 573 K for 3 h. The catalysts obtained from different supports were denoted as AC-CZ, AC-APS-CZ and AC-HNO_3-CZ, respectively. The details of the CZA were described in our previous paper [10].

2.3. Characterization of AC supports and catalysts

Powder X-ray diffraction (XRD) analysis was performed on a Philips PW1130 powder diffractometer with Cu Kα radiation (λ=1.5405 Å) at 40 kV and 25 mA. Nitrogen sorption analysis was measured on a Micromeritics TriStar sorption analyser (USA) and a Micromeritics ASAP 2020 gas adsorption analyser at 77 K. Raman spectra was obtained on a Raman Dilor LabRam-1B microscopic apparatus. I_D and I_G mean the integration of D peak and G peak which located at 1345 and 1589 cm^{-1}, respectively; and I_{TOTAL} means the sum of the interaction of D peak and G peak; R means the ratio of I_D and I_{TOTAL}. XPS was carried out on a Thermo Scientific K-Alpha XPS system (USA). TPR was carried out on a Micromeritics Autochem HP 2950 apparatus. The Cu metal surface area was measured by N_2O chemisorption using a Micromeritics AutoChem HP 2950. The structural features of the produced particles were investigated by TEM on a Philips CM20 and FEI Tecnai F20 at an accelerating voltage of 200 kV. The size and distribution of fine particles were measured using a quantitative image analysis software which was Image-Pro Plus (Media Cybernetics, USA). Using track automatically to measure the particles number and area, then the equivalent particle size was calculated by equal circle processing. Thermal decomposition in O_2 was performed on was conducted on a Mettler Toledo TGA/SDTA851 analyser (Switzerland). Inductively coupled plasma (ICP) was conducted on a Thermo Scientific K-Alpha XPS system.

2.4. Catalytic performance test

Measurements of methanol synthesis activity were conducted in a fixed-bed stainless steel reactor. More details were included in our previous work [10]. One gram of catalysts was reduced in flowing dilute hydrogen (5% H_2 in Ar) at 543 K for 2h. Then methanol synthesis activity was measured at 40 bar and 533 K with the GHSV=3600 h^{-1}. The reactant gas was composed of 25% CO_2 and 75% H_2. Concentrations of the product was analysed using an online refinery gas analyser (Clarus 580 GC; PerkinElmer, USA). Water was removed by cooling the product gas to 272 K. Then analyses were conducted under isothermal conditions at 295 K. Product gas compositions were determined with reference to a series of calibration curves, which were constructed from the analysis of five standard gas mixtures.

3. Results and Discussion

3.1. Physical characterization of AC supports

3.1.1. N_2-physisorption analysis

The nitrogen adsorption isotherms and pore size distributions of various carbon supports were shown in Fig. 1. And the Brunauer-Emmett-Teller (BET) surface area and the porous structure of the supports were summarized in Table 1. Fig. 1a showed that all the supports gave type I isotherms characterized by a plateau that is nearly horizontal to the X-axis. That means all the supports were microporous, which was also shown by the pore size distributions of these supports (Fig. 1b). AC support had a specific surface area of 1146 $m^2\ g^{-1}$ and total pore volume of 0.49 $cm^3\ g^{-1}$. Support AC-APS and AC-HNO_3 had the specific surface of 1046 $m^2\ g^{-1}$ and 753 $m^2\ g^{-1}$ and total pore volume of 0.44 $cm^3\ g^{-1}$ and 0.42 $cm^3\ g^{-1}$, respectively. It is clear that, the specific surface areas and total pore volumes of the modified ACs both decreased after the modifications. This could be either due to the blocking the narrow pores by the functional groups [15,16] or the destruction of the original porosity [13].

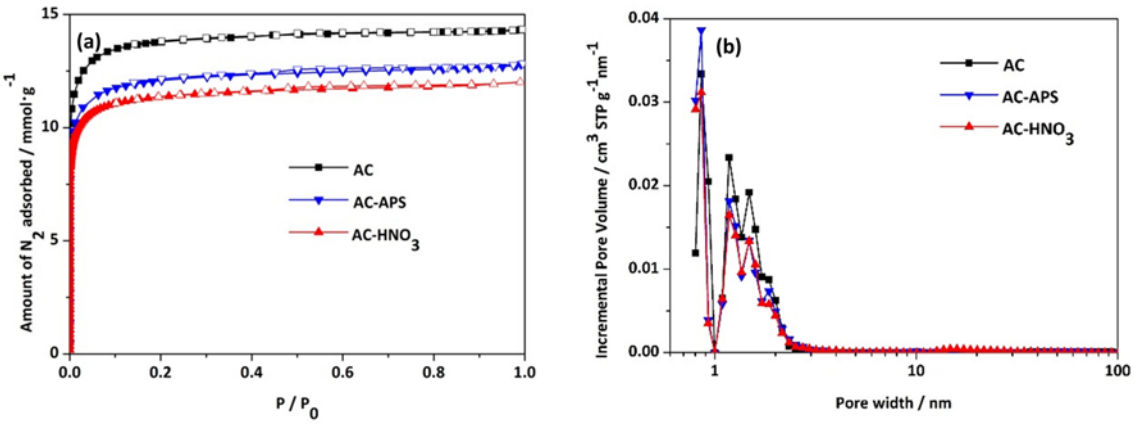

Fig. 1. (a) Isotherms and (b) pore size distributions of support AC, AC-APS and AC-HNO_3 (closed makers represent adsorption data and open markers represent desorption data).

Table 1. Surface area and pore volumes of AC, AC-APS and AC-HNO3

Sample name	BET surface area (m^2 g^{-1})	Pore volume (cm^3 g^{-1})
AC	1146	0.49
AC-APS	1016	0.44
AC-HNO_3	753	0.42

3.1.2. Raman analysis

AC, AC-APS and AC-HNO_3 supports were analysed by a micro-Raman spectroscopy. From Fig. 2a, defect-induced peak (D peak) and graphitic peak (G peak) were detected at 1345 and 1589 cm^{-1}, respectively for all supports. After the spectra were normalised at G peak position, the intensity ratio of D to all peaks in both AC-APS and AC-HNO_3 were higher than AC, implying carbon surface structures contain more defects after the modifications. Of the two modified supports, intensity ratio of D was higher in AC-HNO_3 than AC-APS, suggesting nitric acid modification induced more surface defects than APS. Position and full width at half maximum (FWHM) of D and G peaks had similar values to those typically reported in literature [17]. We also found that there was a relationship between FWHM of D peaks and $R(I_D/I_{TOTAL})$. As shown in Fig. 2b, after AC was modified by means of APS or HNO_3, D peaks were dispersed while $R(I_D/I_{TOTAL})$ increased. This further confirmed that the defected/functionalised sites were introduced on the surface of activated carbon. This result was also in good agreement with the previous studies [18,19].

3.1.3. XPS analysis

The detailed XPS measurements were performed to investigate the chemical characteristics of the C element in the three supports. Fig. 3 showed the C1s XPS analysis of these supports. C1s bonding energies and relative amounts of C in the support were also summarized in Table 2. In the case of AC (Fig. 3a), three peaks appeared at 284.5, 285.3, and 289.5 eV were assigned to the binding energy of C-C, C-O-C and O-C=O bond, respectively [20]. For AC-APS and AC-HNO_3 (Fig. 3b and c), two peaks located at 284.5 and 284.4 eV could be assigned to

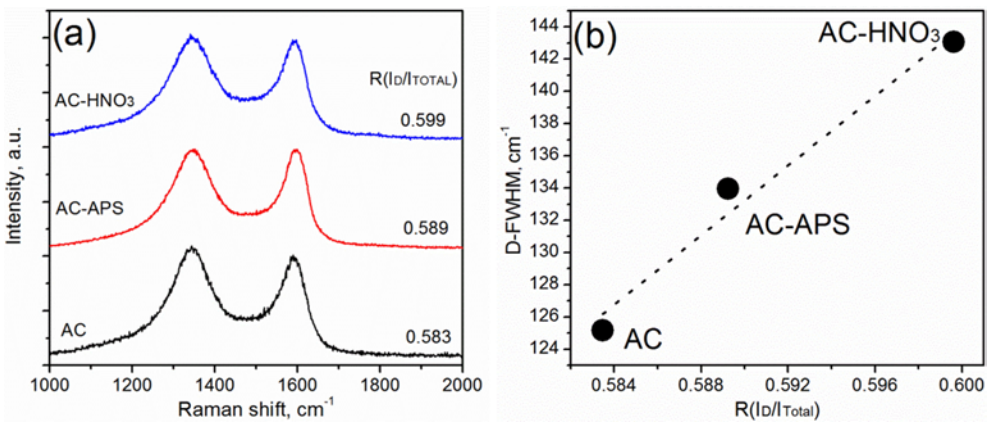

Fig. 2. (a) Raman spectra of AC, AC-APS and AC-HNO_3 samples with the $R(I_D/I_{TOTAL})$; (b) the relationship between $R(I_D/I_{TOTAL})$ and FWHM of D peaks.

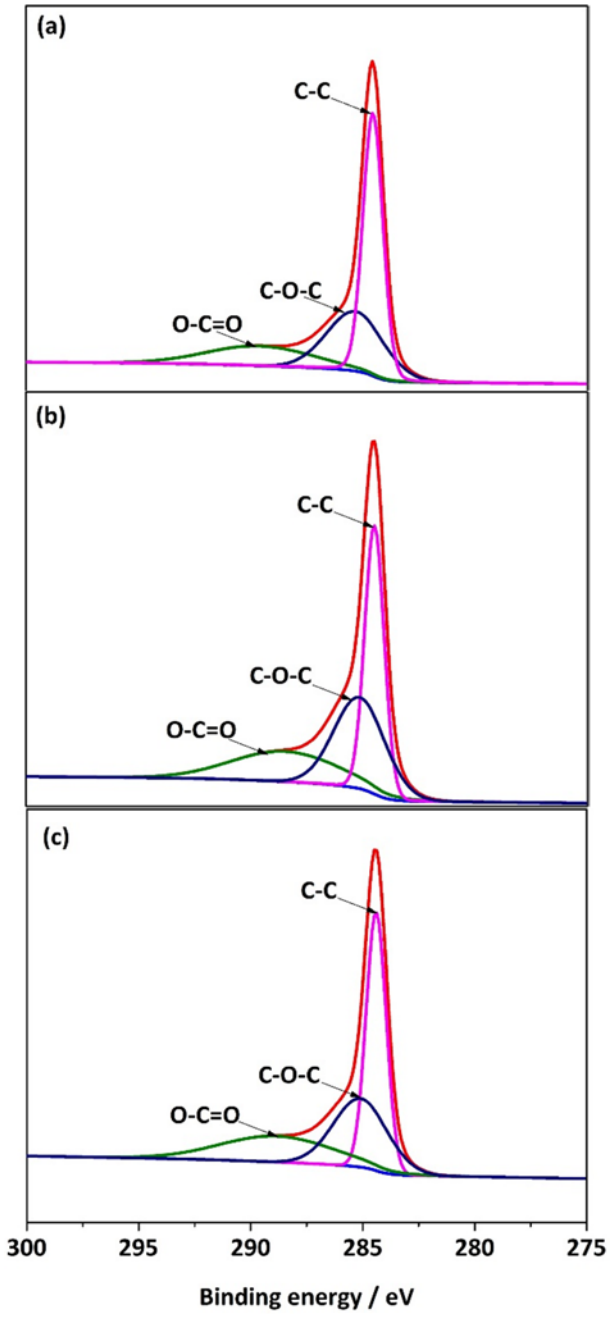

Fig. 3. The XPS spectra of C1s of supports. (a) AC, (b) AC-APS, and (c) AC-HNO_3.

C-C bond; peaks located at 285.1 eV could be assigned to C-O-C bond and peaks located at 288.5 and 288.7 eV were contributed by O-C=O bond. AC support has 39% of C-C bond, 33% of C-O-C, and 28% of O-C=O. While AC-APS support has 36% of C-C bond, 34% of C-O-C, and 30% of O-C=O. And AC-HNO_3 support has 37% of C-C bond, 33% of C-O-C, and 30% of O-C=O. Comparing the relative amount of the bond in the three supports, it is clear that, the C-C bond in AC support was more than that in AC-APS support and AC-HNO_3 support. AC support has less C-O-C and O-C=O bonds compared to AC-APS and AC-HNO_3. That means the C-C bond was oxidized to C-O-C or O-C=O during the modifications.

3.1.4. Morphology and structural analysis

TEM images of the three supports were presented in Fig. 4a-c, respectively. The TEM diffraction pattern of the blank AC (inset of Fig. 4a) showed transformed spots meaning that AC had some impurities. For modified supports, AC-APS and AC-HNO_3, there were no transformed spot (their insets of Fig. 4b and c) in their diffraction pattern, suggesting that after the APS or HNO_3 treatment, the impurities have been removed. It is worth mentioning that the diffraction images of the two acid treated supports showed diffraction rings though with weakened strength, suggesting that the carbon structures having changed from amorphous to slightly graphitic. These results were in good agreement with the Raman results (see 3.1.2).

3.1.5. Thermogravimetric analysis

Thermal decomposition data of the supports AC, AC-APS and AC-HNO_3 were presented in Fig. 5. It showed that the weight loss the original AC was negligible when the temperature was lower than 750 K. The maximum weight loss of AC appeared in the range of 750–850 K. When the temperature was lower than 800 K, support AC-APS had about 15% weight loss, with its maximum weight loss appeared in the range of 800–950 K, suggesting more stable carbon structure. For support AC-HNO_3, the low temperature weight loss was similar to that of support AC-APS up to 600 K, which was believed to be the release or decomposition of the functional groups generated from the APS or HNO_3 modifications. Major weight loss happened around 700 K which was lower than the other two supports, suggesting the existence of less stable structure. There was another weight loss between 750 K and 900 K, which was higher than the original carbon and could be related to more ordered structure introduced by the HNO_3 treatment. Comparing the maximum weight loss tem-

Table 2. C1s binding energies, relative amounts of bond in each spectrum

Spectra	Binding energy (eV); relative amount (%)[a]			Assignment of the components
	AC	AC-APS	AC-HNO_3	
C1s	284.5; 39	284.5; 36	284.4; 37	C-C
	285.3; 33	285.1; 34	285.1; 33	C-O-C
	289.5; 28	288.5; 30	288.7; 30	O-C=O

[a]Relative amount was calculated from the relative area ratio of each peak.

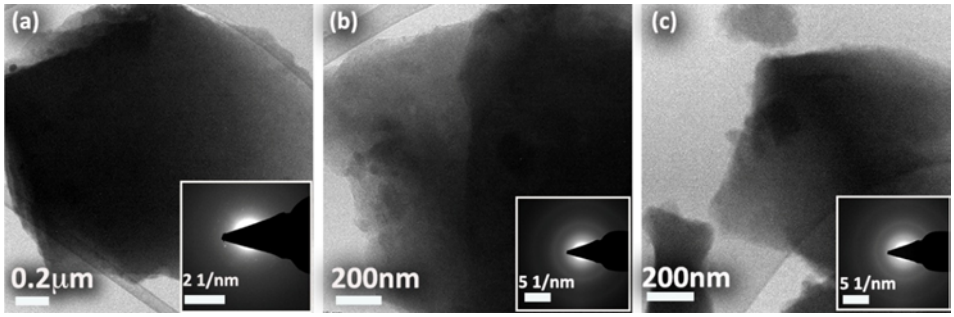

Fig. 4. TEM images of supports. (a) AC, (b) AC-APS, and (c) AC-HNO_3.

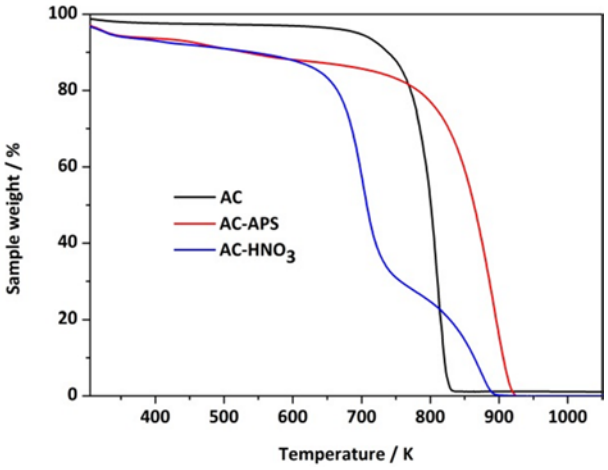

Fig. 5. TG curves of supports AC, AC-APS and AC-HNO_3.

peratures of the three samples, it can be concluded that, APS modification enhanced the thermal stability of AC support. HNO_3 modification caused structures changes in two-fold, one of which made the support less thermal stable than original AC and the other made it more thermal stable.

3.2. Physical characterization of catalysts

3.2.1. N_2-physisorption analysis

The nitrogen adsorption isotherms and pore size distributions of the prepared catalysts were shown in Fig. 6. The BET surface area and porous structure of the catalysts were summarized in Table 3. First of all, all the catalysts still gave type I isotherms indicating they were maintaining microporous nature but showed significantly decreased BET surface areas and pore volumes compared to their corresponding supports (Fig. 1a). It has small amount of meso-pores in the catalysts as well (Fig. 6). Catalyst AC-CZ had a BET surface area of 641 $m^2\ g^{-1}$ and a pore volume of 0.30 $cm^3\ g^{-1}$. AC-APS-CZ had a BET surface area of 594 $m^2\ g^{-1}$ and a pore volume of 0.28 $cm^3\ g^{-1}$, while AC-HNO_3-

Table 3. BET surface area and pore volume of the prepared catalysts

Sample name	BET surface area ($m^2\ g^{-1}$)	Pore volume ($cm^3\ g^{-1}$)
AC-CZ	641	0.30
AC-APS-CZ	594	0.28
AC-HNO_3-CZ	658	0.30

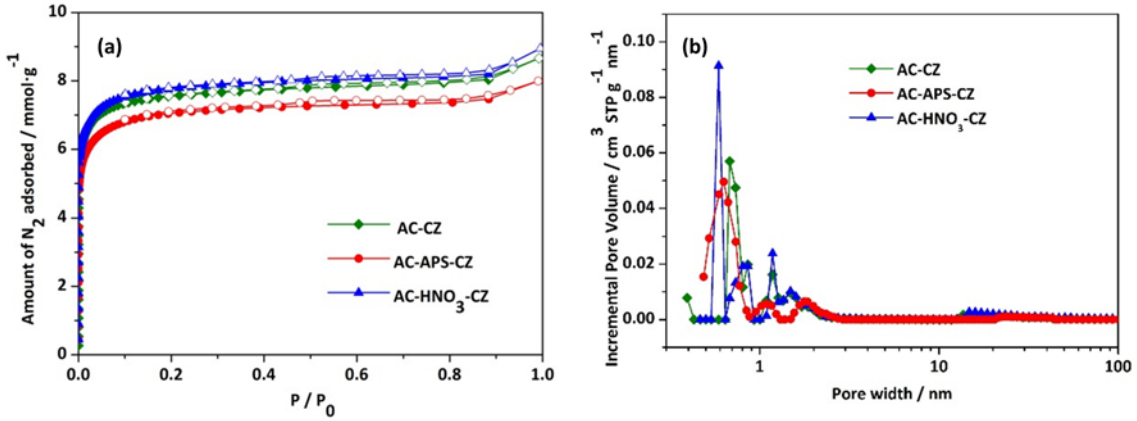

Fig. 6. (a) Isotherms and (b) pore size distributions of catalysts AC-CZ, AC-APS-CZ and AC-HNO_3-CZ (closed makers represent adsorption data and open markers represent desorption data).

CZ had a BET surface area of 658 m^2 g^{-1} and the same pore volume as AC-CZ. It is clear that all the results and catalysts have reduced BET surface area and pore volume because introduce of copper and zinc oxides in the carbon supports has taken up the space in the carbon supports.

3.2.2. XRD analysis

XRD patterns of the three prepared catalysts were presented in Fig. 7. All these three catalysts showed a very broad peak at about 2θ=24°, indicating the nature of the amorphous carbon support. For catalyst AC-CZ, there were three peaks indexed to CuO (PDF No. 78-428 and 80-1916) (Fig. 7a), which came from the decomposition of copper nitrate precursor. The other three peaks were indexed to Cu_2O (PDF No. 1-1142), suggesting some of the CuO was reduced to some degree by carbon. For catalyst AC-APS-CZ, the intensity of the Cu_2O peaks were much stronger than those in catalyst AC-CZ, indicating a better crystalline of Cu_2O generated in the catalyst, which could be caused by the strong reduction environment in this catalyst. Furthermore, there was a Cu (PDF No. 85-1326) peak appearing in this catalyst, further confirming the more reducibility of this catalyst. As for catalyst AC-HNO_3-CZ, all the main peaks were indexed to Cu_2O (PDF No. 1-1142) with almost no detection of CuO, suggesting all CuO had been reduced to Cu_2O form. The above results helped us to conclude that both modification methods have changed the surface property of the original activated carbon, which further facilitated the reduction of CuO in the subsequent processes. Our findings were also in agreement with the literature [21], which suggested that, HNO_3 treatment and APS treatment changed the surface functional groups on carbon substrate and therefore changed the interaction between the metal precursor and the carbon supports, and affected the reduction of the Cu species [22] by the carbon support in the subsequent calcinations step. No crystalline ZnO was detected among all the three catalysts indicating either ZnO crystalline was too small or amorphous in these catalysts.

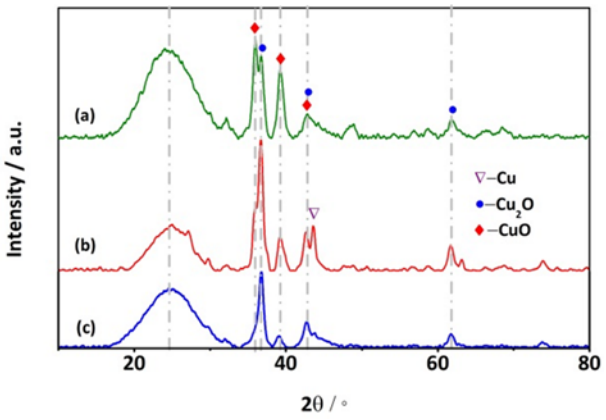

Fig. 7. XRD spectra of catalysts. (a) AC-CZ, (b) AC-APS-CZ, and (c) AC-HNO_3-CZ.

3.2.3. XPS analysis

The detailed XPS measurements were performed to investigate the chemical characteristics of the Cu element in the three catalysts. Fig. 8 showed the Cu 2p XPS analysis of the catalysts. Cu2p bonding energies and relative amounts of Cu in the catalysts were also summarized in Table 4. In the case of AC-CZ (Fig. 8a), one peak appeared at 933.0 and the extra shake-up satellite peaks were assigned to the binding energy of Cu 2p3/2 and Cu 2p1/2, respectively, indicating the presence of the Cu^{2+} in the sample [23,24]. For AC-APS-CZ and AC-HNO_3-CZ (Fig. 8b and c), two peaks located at 931.1 eV and 932.85±0.05 eV could

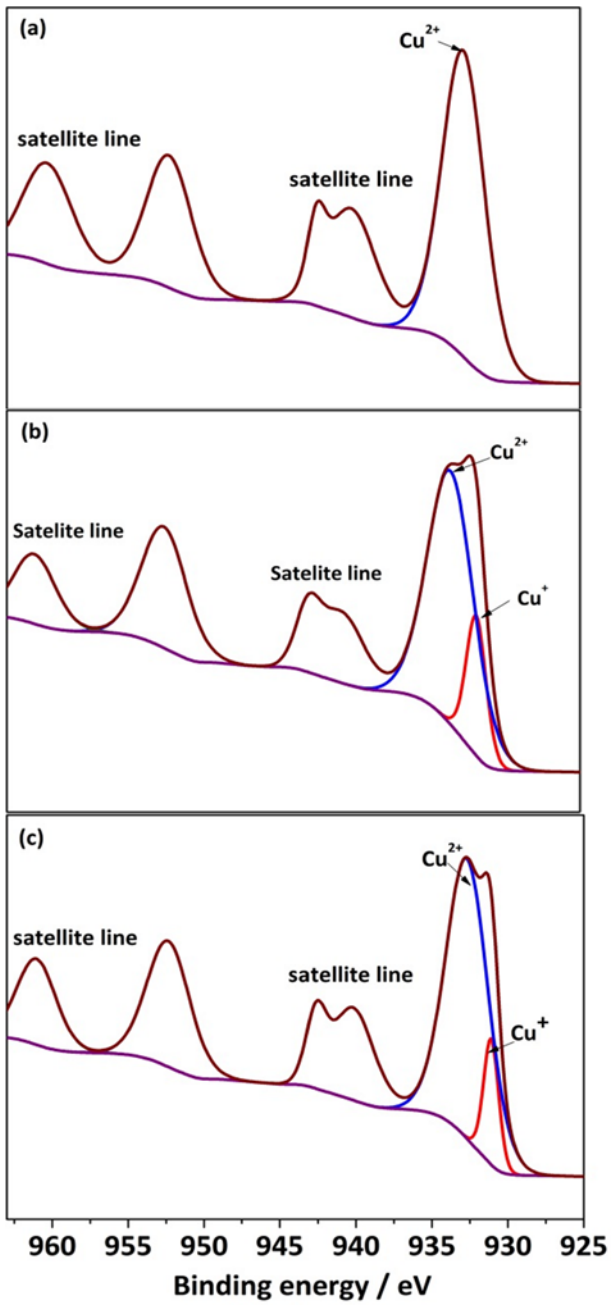

Fig. 8. The XPS spectra of Cu2p of catalysts. (a) AC-CZ, (b) AC-APS-CZ, and (c) AC-HNO_3-CZ.

Table 4. Cu2p binding energies, relative amounts of Cu in each spectrum

Spectra	Binding energy (eV); relative amount (%)[a]			Assignment of the components
	AC-CZ	AC-APS-CZ	AC-HNO_3-CZ	
Cu2p	-	931.1; 19	931.1; 14	Cu^+
	933.0; 100	932.9; 81	932.8; 86	Cu^{2+}

[a]Relative amount was calculated from the relative area ratio of each peak.

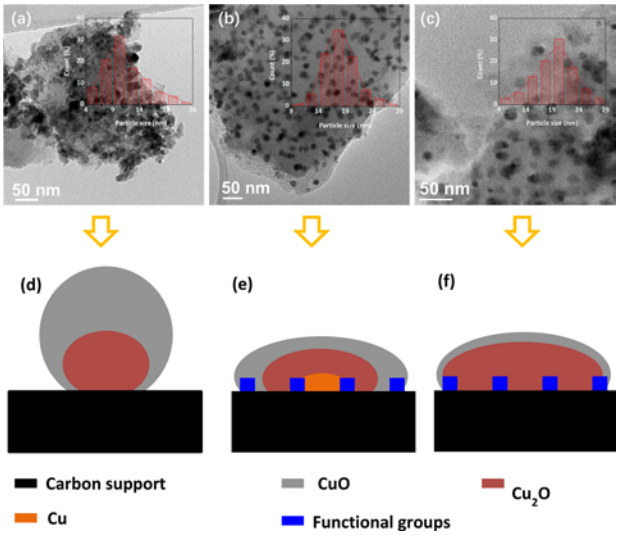

Fig. 9. TEM images of sample: (a) AC-CZ; (b) AC-APS-CZ; (c) AC-HNO_3-CZ; and schematic graphs of sample: (d) AC-CZ; (e) AC-APS-CZ; (f) AC-HNO_3-CZ.

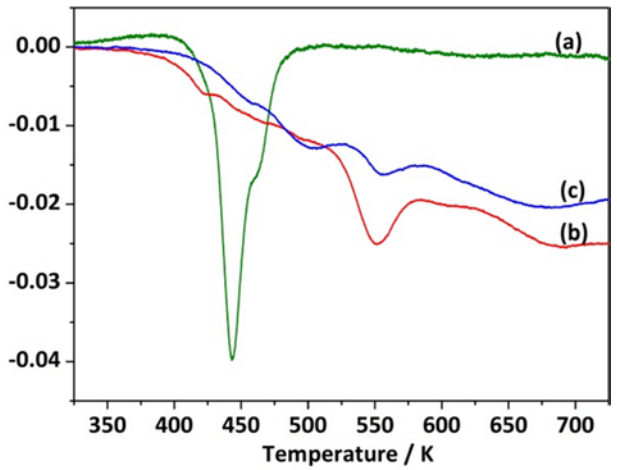

Fig. 10. TPR profiles of catalysts. (a) AC-CZ, (b) AC-APS-CZ, and (c) AC-HNO_3-CZ.

be assigned to Cu^+ and Cu^{2+}, respectively [25].

We have to point out that these XPS results are slightly different from our XRD results. The main reason is because XPS is more like a surface technique, normally can detect features in several nano-meters in depth. The reason that XRD was not able to detect the different chemical states as observed by XPS could be those chemical states were the very thin layers outside the core metal oxides. Therefore, the difference in XRD and XPS could help us to suggest a core-shell Cu related species grown on the carbon support. For AC-CZ, the Cu species was consisting of an outer layer of CuO and the Cu_2O core. For AC-APS-CZ, it had a Cu core, a middle layer of Cu_2O and an outer layer of CuO. As for AC-HNO_3-CZ, there was still some CuO remaining on the outer layer of the Cu_2O which might have been re-oxidised and stayed in the outer layer of the catalysts. The schematic pictures were shown in Fig. 9d-f.

3.2.4. Temperature programmed reduction

To investigate the reduction behavior of the catalysts, TPR measurements were performed and the results were shown in Fig. 10. It was observed that AC-CZ catalyst exhibited a sharp reduction peak at around 440 K with a shoulder peak at about 460 K. The former peak could be assigned to the reduction of Cu^{2+} to Cu^+ and the later one is to the stepwise reduction of Cu^+ ions to Cu^0 according to the literature [26]. Catalyst AC-APS-CZ and AC-HNO_3-CZ had similar TPR profiles, which started reduction at around 400 K and showed a small peak at 550 K. The reduction temperature of Cu in sample AC-APS-CZ and AC-HNO_3-CZ were much higher than that of AC-CZ, indicating the CuO was more difficult to reduce and suggesting there is stronger metal and support interaction between the catalyst and the support. As is known in literatures [27,28], the reduction temperature is attributed to the metal-support interaction. Strong metal-support interaction corresponds to higher reduction temperature. When the support was modified with APS or HNO_3, it created more functional groups on the support surface to act as anchors for the metal to bind. Thus, it is understandable that AC-APS-CZ and AC-HNO_3-CZ had much stronger metal-support interactions than AC-CZ. So the reduction temperature shifted to higher temperature ranges. It is worth noting that, the reduction of all these three catalysts started at almost the same temperature. But the Cu^+ reduction peak dramatically shifted to higher temperature in the catalysts AC-APS-CZ and AC-HNO_3-CZ, suggesting the binding sites for Cu^{2+} was similar in all catalysts. Considering the Cu^{2+} was always at the outer layer, the interaction of metal and support had minimum effect on its reduction property, leading to our subsequent observation that reduction temperature for Cu^{2+} was always at similar temperature. Also, it should be noticed that, for AC-CZ, in the temperature range of 500 K and above (mainly related to reduction of Cu^+ to Cu^0), the amount of consumed H_2 was negligible. While for AC-APS-CZ and AC-HNO_3-CZ, the consumed H_2 were still very high, suggesting a large amount of the Cu species were reduced in the range of 600–725 K by H_2 because of the stronger interaction with the support.

Table 5. Metal loading, Cu surface area and catalytic performances of the catalysts

Catalyst name	CuO-ZnO (%)[a]	Cu (%)[b]	Zn (%)[b]	Cu-SA (m^2 g^{-1})	MTY (mmol-CH_3OH/(g-cat·h))[c]	MTY (mmol-CH_3OH/(g-Cu·h))[d]
AC-CZ	21.9	14.8	8.9	18.6	3.1	23
AC-APS-CZ	21.0	13.2	8.8	2.3	0.2	2
AC-HNO_3-CZ	19.0	11.4	6.3	1.0	0.2	2
CZA	-	61.6	28.0	35.2	5.6	9

[a]Obtained from TGA tests.
[b]Obtained from ICP tests.
[c]Mass-time yield per gram of catalyst.
[d]Mass-time yield per gram of Cu loading.

3.2.5. Morphology and structural analysis

TEM micrographs of the catalysts were shown in Fig. 9. Catalyst AC-CZ showed randomly dispersed metal/metal oxide in the support (Fig. 9a). The metal/metal oxides sizes were around 10 nm (Fig. 9a inset). For catalyst AC-APS-CZ, uniform metal oxide particles well dispersed in the support (Fig. 9b and inset). Similar metal dispersion could be seen for the catalyst AC-HNO_3-CZ (Fig. 9c and inset). Fig. 9b and c insets showed that these metal oxides are around 20 nm. The particle sizes were larger in the catalysts AC-APS-CZ and AC-HNO_3-CZ than that in AC-CZ. For these two catalysts, the modifications created functional groups on the carbon surface, thus, increased the wettability of the supports. These particles spread in the support as wide as possible and firmly "grew" in the support. It also explained the much stronger metal-support interactions on these two catalysts. This result is in agreement with the literatures [29,30]. Both modification methods created acidic oxygen surface groups that increased the hydrophilicity of the carbon supports. A better wettability of the more hydrophilic AC-APS and AC-HNO_3 supports led to much stronger metal-support interactions in the sample AC-APS-CZ and AC-HNO_3-CZ. Sample AC-CZ (Fig. 9d) had the smallest metal-support interaction among these three samples due to its hydrophobic nature and with the CuO partially reduced to Cu_2O. AC-CZ might have a Cu_2O-CuO core-shell structure which could be deduced from the XRD and XPS results. Catalyst AC-CZ Sample AC-APS-CZ (Fig. 9e) had stronger metal-support interaction than sample AC-CZ, leading to the further reduction of Cu species. In this case, a Cu-Cu_2O-CuO core-shell structure was formed which could be deduced from their corresponding XRD and XPS results as well. For catalyst AC-HNO_3-CZ, the structure may be a Cu_2O-CuO core-shell structure with most of the Cu species in the Cu^+ form. From the TEM results, it could be concluded that, the APS or HNO_3 modification will generate much stronger metal-support interactions of resulted catalysts which is in agreement with the literature [31].

3.3. Catalytic performance tests

The metal loading, Cu surface area and methanol synthesis activity results over the prepared catalysts were summarized in Table 5. The metal loading, Cu surface area and methanol synthesis activity of the three supports were also tested under the same conditions. The methanol yields were negligible. The metal loading of the three prepared catalysts were in the range of 19.0% to 21.9% which were close to the theoretical value. The ICP results showed that the Cu-Zn ratio of prepared were all less than the designed ratio 2, which was 1.66 for catalyst AC-CZ, 1.50 for AC-APS-CZ and 1.81 for AC-HNO_3-CZ, respectively. While for CZA, the Cu-Zn ratio was 2.2. The Cu surface area was significantly different among these for catalysts. Catalyst AC-CZ had a Cu surface area of 18.6 m^2 g^{-1} and catalyst AC-APS-CZ had a Cu surface area of 2.3 m^2 g^{-1}. As for catalyst AC-HNO_3-CZ, it had a Cu surface area of 1.0 m^2 g^{-1}. For CZA, it had a Cu surface area of 35.2 m^2 g^{-1}. With similar Cu loading amount as shown by our TGA tests results for the prepared catalysts, the Cu surface area of AC-CZ was 8 times as much as that of catalyst AC-APS-CZ and 18 times as much as that of AC-HNO_3-CZ. This is because the Cu surface area was measured by the N_2O reactive frontal chromatography method in this work. For this measurement, H_2 gas was introduced to reduce Cu^{2+} to Cu^0 at 543 K, then N_2O gas was used to oxidise Cu^0 to Cu^+. Meanwhile, N_2O was reduced to N_2 [32,33]. The generated N_2 amount was used to determine the Cu surface area. This could be expressed as Eq. 1.

$$N_2O_{(g)} + 2Cu^0 \rightarrow N_{2(g)} + 2Cu^+ + O^{2-} \quad (1)$$

From the TPR results, below 550 K, only a small portion of Cu^{2+} was reduced to Cu^+, even smaller amount of Cu^+ was reduced to Cu^0 in the catalyst AC-APS-CZ and AC-HNO_3-CZ. In this case, very little amount of N_2 will be detected by the end. As a result, the detected Cu surface areas were very low for catalysts AC-APS-CZ and AC-HNO_3-CZ. This also explained why these two catalysts had disappointing catalytic performances, which were only 0.2 mmol-CH_3OH/(g-cat·h). Methanol production results have indicated that catalyst CZA produced the most methanol with MTY of 5.6 mmol-CH_3OH/(g-cat·h) and AC-CZ produced a methanol rate of 3.1 mmol-CH_3OH/(g-cat·h). It is worthy notice that, Catalyst CZA had a Cu loading of 61.6% while AC-CZ only had a Cu loading of 14.8%. So AC-CZ had a methanol formation rate of 23 mmol-CH_3OH/(g-Cu·h) while CZA was 9 mmol-CH_3OH/(g-cat·h). Which means, on a Cu loading basis, AC-CZ was 2.6 times as active as CZA.

The above results led us to conclude that the modification methods have huge influences on metal-support interaction. Cat-

alysts with modifications have the anchor sites to generate stronger metal-support interaction than the catalyst without modification. This leads to much higher reduce temperature of the CuO particles and very disappointing activity. While AC-CZ catalyst has even better activity than the CZA on a Cu loading basis due to the promotion effect of carbon support.

4. Conclusions

Catalysts containing Cu and ZnO on the activated carbon and modified activated carbon surfaces were achieved active for methanol synthesis from CO_2 hydrogenation, in particular activated carbon supported catalyst AC-CZ is more active catalyst than a CZA on a Cu loading basis, suggesting that the carbon support without any modification could promt the catalyst activity. Both modification methods created strong metal-support interactions which made CuO more difficult to reduce, leading to the much less activity of the resulted catalysts (AC-APS-CZ and AC-HNO_3-CZ).

Conflict of Interest

No potential conflict of interest relevant to this article was reported.

Acknowledgements

HD is grateful for financial support provided by the National Natural Science Foundation of China(no. 51704048) and the scientific research start-up funding from Chongqing University.

References

[1] Olah GA, Goeppert A, Prakash GKS. Chemical recycling of carbon dioxide to methanol and dimethyl ether: from greenhouse gas to renewable, environmentally carbon neutral fuels and synthetic hydrocarbons. J Org Chem, **74**, 487 (2009). https://doi.org/10.1021/jo801260f.

[2] Pan YX, Liu CJ, Ge Q. Effect of surface hydroxyls on selective CO_2 hydrogenation over Ni_4/γ-Al_2O_3: a density functional theory study. J Catal, **272**, 227 (2010). https://doi.org/10.1016/j.jcat.2010.04.003.

[3] da Silva RJ, Pimentel AF, Monteiro RS, Mota CJA. Synthesis of methanol and dimethyl ether from the CO_2 hydrogenation over Cu·ZnO supported on Al_2O_3 and Nb_2O_5. J CO_2 Util, **15**, 83 (2016). https://doi.org/10.1016/j.jcou.2016.01.006.

[4] Twigg MV, Spencer MS. Deactivation of copper metal catalysts for methanol decomposition, methanol steam reforming and methanol synthesis. Top Catal, **22**, 191 (2003). https://doi.org/10.1023/A:1023567718303.

[5] Waugh KC. Methanol synthesis. Catal Today, **15**, 51 (1992). https://doi.org/10.1016/0920-5861(92)80122-4.

[6] Klier K. Methanol synthesis. Adv Catal, **31**, 243 (1982). https://doi.org/10.1016/S0360-0564(08)60455-1.

[7] Zhang Y, Zhong L, Wang H, Gao P, Li X, Xiao S, Ding G, Wei W, Sun Y. Catalytic performance of spray-dried Cu/ZnO/Al_2O_3/ZrO_2 catalysts for slurry methanol synthesis from CO_2 hydrogenation. J CO_2 Util, **15**, 72 (2016). https://doi.org/10.1016/j.jcou.2016.01.005.

[8] Zhou J, Tsai HL. Effects of electromagnetic force on melt flow and porosity prevention in pulsed laser keyhole welding. Int J Heat Mass Transfer, **50**, 2217 (2007). https://doi.org/10.1016/j.ijheatmasstransfer.2006.10.040.

[9] Yang Y, Brown CM, Zhao C, Chaffee AL, Nick B, Zhao D, Webley PA, Schalch J, Simmons JM, Liu Y, Her JH, Buckley CE, Sheppard DA. Micro-channel development and hydrogen adsorption properties in templated microporous carbons containing platinum nanoparticles. Carbon, **49**, 1305 (2011). https://doi.org/10.1016/j.carbon.2010.11.050.

[10] Duan H, Yang Y, Singh R, Chiang K, Wang S, Xiao P, Patel J, Danaci D, Burke N, Zhai Y, Webley PA. Mesoporous carbon-supported Cu/ZnO for methanol synthesis from carbon dioxide. Aust J Chem, **67**, 907 (2014). https://doi.org/10.1071/ch13622.

[11] Duan H, Yang Y, Patel J, Dumbre D, Bhargava SK, Burke N, Zhai Y, Webley PA. A facile method to synthesis a mesoporous carbon supported methanol catalyst containing well dispersed Cu/ZnO. Mater Res Bull, **60**, 232 (2014). https://doi.org/10.1016/j.materresbull.2014.08.007.

[12] Roberts IA, Wang CJ, Esterlein R, Stanford M, Mynors DJ. A three-dimensional finite element analysis of the temperature field during laser melting of metal powders in additive layer manufacturing. Int J Mach Tools Manuf, **49**, 916 (2009). https://doi.org/10.1016/j.ijmachtools.2009.07.004.

[13] Calafat A, Laine J, López-Agudo A, Palacios JM. Effect of surface oxidation of the support on the thiophene hydrodesulfurization activity of Mo, Ni, and NiMo catalysts supported on activated carbon. J Catal, **162**, 20 (1996). https://doi.org/10.1006/jcat.1996.0256.

[14] Aksoylu AE, Madalena M, Freitas A, Pereira MFR, Figueiredo JL. The effects of different activated carbon supports and support modifications on the properties of Pt/AC catalysts. Carbon, **39**, 175 (2001). https://doi.org/10.1016/s0008-6223(00)00102-0.

[15] Shim JW, Park SJ, Ryu SK. Effect of modification with HNO_3 and NaOH on metal adsorption by pitch-based activated carbon fibers. Carbon, **39**, 1635 (2001). https://doi.org/10.1016/s0008-6223(00)00290-6.

[16] Aggarwal D, Goyal M, Bansal RC. Adsorption of chromium by activated carbon from aqueous solution. Carbon, **37**, 1989 (1999). https://doi.org/10.1016/s0008-6223(99)00072-x.

[17] Cuesta A, Dhamelincourt P, Laureyns J, Martínez-Alonso A, Tascón JMD. Raman microprobe studies on carbon materials. Carbon, **32**, 1523 (1994). https://doi.org/10.1016/0008-6223(94)90148-1.

[18] Milone C, Hameed ARS, Piperopoulos E, Santangelo S, Lanza M, Galvagno S. Catalytic wet air oxidation of p-coumaric acid over carbon nanotubes and activated carbon. Ind Eng Chem Res, **50**, 9043 (2011). https://doi.org/10.1021/ie200492g.

[19] Motchelaho MAM, Xiong H, Moyo M, Jewell LL, Coville NJ. Effect of acid treatment on the surface of multiwalled carbon nanotubes prepared from Fe–Co supported on $CaCO_3$: correlation with Fischer–Tropsch catalyst activity. J Mol Catal A Chem, **335**, 189 (2011). https://doi.org/10.1016/j.molcata.2010.11.033.

[20] Shchukarev A, Korolkov D. XPS study of group IA carbonates. Open Chem, **2**, 347 (2004). https://doi.org/10.2478/BF02475578.

[21] Chuang KH, Lu CY, Wey MY, Huang YN. NO removal by activated carbon-supported copper catalysts prepared by impregnation,

polyol, and microwave heated polyol processes. Appl Catal A Gen, **397**, 234 (2011). https://doi.org/10.1016/j.apcata.2011.03.003.

[22] Chen JP, Wu S, Chong KH. Surface modification of a granular activated carbon by citric acid for enhancement of copper adsorption. Carbon, **41**, 1979 (2003). https://doi.org/10.1016/s0008-6223(03)00197-0.

[23] Zhang Z, Wang P. Highly stable copper oxide composite as an effective photocathode for water splitting via a facile electrochemical synthesis strategy. J Mater Chem, **22**, 2465 (2012). https://doi.org/10.1039/c1jm14478b.

[24] Liu P, Hensen EJM. Highly efficient and robust Au/$MgCuCr_2O_4$ catalyst for gas-phase oxidation of ethanol to acetaldehyde. J Am Chem Soc, **135**, 10432 (2013). https://doi.org/10.1021/ja406820f.

[25] Hawaldar R, Merino P, Correia MR, Bdikin I, Grácio J, Méndez JG, Martín-Gago JA, Singh MK. Large-area high-throughput synthesis of monolayer graphene sheet by hot filament thermal chemical vapor deposition. Sci Rep, **2**, 682 (2012). https://doi.org/10.1038/srep00682.

[26] Redina EA, Greish AA, Mishin IV, Kapustin GI, Tkachenko OP, Kirichenko OA, Kustov LM. Selective oxidation of ethanol to acetaldehyde over Au–Cu catalysts prepared by a redox method. Catal Today, **241**, 246 (2015). https://doi.org/10.1016/j.cattod.2013.11.065.

[27] de Llobet S, Pinilla JL, Moliner R, Suelves I. Effect of the synthesis conditions of Ni/Al_2O_3 catalysts on the biogas decomposition to produce H_2-rich gas and carbon nanofibers. Appl Catal B Environ, **165**, 457 (2015). https://doi.org/10.1016/j.apcatb.2014.10.014.

[28] Xiao J, Mao D, Guo X, Yu J. Methanol synthesis from CO_2 hydrogenation over CuO-ZnO-TiO_2 catalysts: the influence of TiO_2 content. Energy Technol, **3**, 32 (2015). https://doi.org/10.1002/ente.201402091.

[29] Prado-Burguete C, Linares-Solano A, Rodríguez-Reinoso F, de Lecea CSM. The effect of oxygen surface groups of the support on platinum dispersion in Pt/carbon catalysts. J Catal, **115**, 98 (1989). https://doi.org/10.1016/0021-9517(89)90010-9.

[30] Noh JS, Schwarz JA. Effect of HNO_3 treatment on the surface acidity of activated carbons. Carbon, **28**, 675 (1990). https://doi.org/10.1016/0008-6223(90)90069-b.

[31] Martin O, Mondelli C, Curulla-Ferré D, Drouilly C, Hauert R, Pérez-Ramírez J. Zinc-rich copper catalysts promoted by gold for methanol synthesis. ACS Catal, **5**, 5607 (2015). https://doi.org/10.1021/acscatal.5b00877.

[32] Chinchen GC, Hay CM, Vandervell HD, Waugh KC. The measurement of copper surface areas by reactive frontal chromatography. J Catal, **103**, 79 (1987). https://doi.org/10.1016/0021-9517(87)90094-7.

[33] Scholten JJF, Konvalinka JA. Reaction of nitrous oxide with copper surfaces: application to the determination of free-copper surface areas. Trans Faraday Soc, **65**, 2465 (1969). https://doi.org/10.1039/tf9696502465.